

# UC Berkeley

## UC Berkeley Previously Published Works

### Title

X-Ray absorption spectroscopy of LiBF<sub>4</sub> in propylene carbonate: a model lithium ion battery electrolyte

### Permalink

<https://escholarship.org/uc/item/0k9486t0>

### Journal

Physical Chemistry Chemical Physics, 16(43)

### ISSN

0956-5000

### Authors

Smith, Jacob W  
Lam, Royce K  
Sheardy, Alex T  
[et al.](#)

### Publication Date

2014-11-21

### DOI

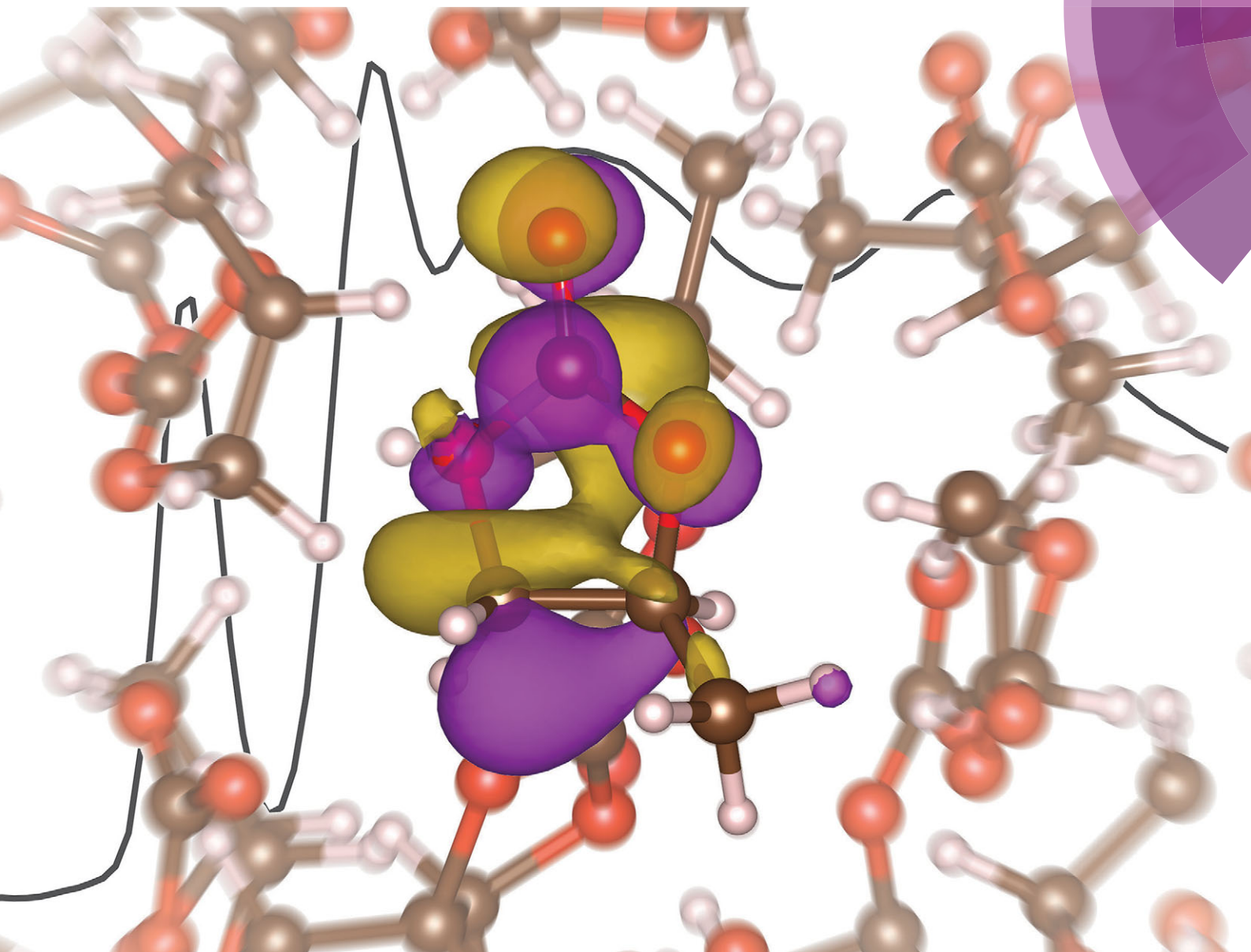
10.1039/c4cp03240c

Peer reviewed

# PCCP

Physical Chemistry Chemical Physics

[www.rsc.org/pccp](http://www.rsc.org/pccp)



ISSN 1463-9076



**PAPER**

Richard J. Saykally *et al.*

X-Ray absorption spectroscopy of  $\text{LiBF}_4$  in propylene carbonate: a model lithium ion battery electrolyte



Cite this: *Phys. Chem. Chem. Phys.*,  
2014, **16**, 23568

# X-Ray absorption spectroscopy of LiBF<sub>4</sub> in propylene carbonate: a model lithium ion battery electrolyte†

Jacob W. Smith,<sup>ab</sup> Royce K. Lam,<sup>ab</sup> Alex T. Sheardy,<sup>ab</sup> Orion Shih,<sup>a</sup>  
Anthony M. Rizzuto,<sup>a</sup> Oleg Borodin,<sup>c</sup> Stephen J. Harris,<sup>d</sup> David Prendergast<sup>e</sup> and  
Richard J. Saykally<sup>\*ab</sup>

Since their introduction into the commercial marketplace in 1991, lithium ion batteries have become increasingly ubiquitous in portable technology. Nevertheless, improvements to existing battery technology are necessary to expand their utility for larger-scale applications, such as electric vehicles. Advances may be realized from improvements to the liquid electrolyte; however, current understanding of the liquid structure and properties remains incomplete. X-ray absorption spectroscopy of solutions of LiBF<sub>4</sub> in propylene carbonate (PC), interpreted using first-principles electronic structure calculations within the eXcited electron and Core Hole (XCH) approximation, yields new insight into the solvation structure of the Li<sup>+</sup> ion in this model electrolyte. By generating linear combinations of the computed spectra of Li<sup>+</sup>-associating and free PC molecules and comparing to the experimental spectrum, we find a Li<sup>+</sup>-solvent interaction number of 4.5. This result suggests that computational models of lithium ion battery electrolytes should move beyond tetrahedral coordination structures.

Received 22nd July 2014,  
Accepted 19th August 2014

DOI: 10.1039/c4cp03240c

www.rsc.org/pccp

## Introduction

Lithium ion batteries (LIBs) have rapidly grown to dominate the rechargeable battery market for portable technology. Given the simultaneous expansion of the market for handheld devices (*i.e.* cellular phones, laptops, tablets, *etc.*), LIBs now comprise a multibillion dollar industry.<sup>1</sup> Such demand has spurred intense research and development efforts.<sup>2</sup> Nevertheless, serious shortcomings persist which limit the utility of modern LIBs for larger-scale applications in electric vehicles (EVs) or for power storage utilized in conjunction with intermittent renewable energy sources (wind, solar, *etc.*).<sup>2–4</sup> These shortcomings include high cost, energy density below optimal EV standards, slow recharging rates, and limited lifetimes.

A typical commercial LIB consists of a graphite negative electrode and metal oxide or metal phosphate positive electrode (*e.g.* LiCoO<sub>2</sub>, LiFePO<sub>4</sub>, LiMnO<sub>2</sub>, *etc.*). Charge is transported by lithium ions travelling between the electrodes through a liquid electrolyte commonly consisting of a lithium salt with a large, charge-disperse anion such as PF<sub>6</sub><sup>−</sup>, BF<sub>4</sub><sup>−</sup>, ClO<sub>4</sub><sup>−</sup>, or more recently larger, carbon-based anions such as bis(oxalato)borate {B(C<sub>2</sub>O<sub>4</sub>)<sub>2</sub><sup>−</sup>; BOB<sup>−</sup>} dissolved in a non-aqueous solvent. These solvents typically consist of combinations of linear alkyl carbonate molecules such as dimethyl carbonate (DMC) and ethyl methyl carbonate (EMC), and the cyclic alkyl carbonate ethylene carbonate (EC). Propylene carbonate (PC), a structural analogue of EC with a methyl group on a ring carbon, is unsuitable for use in commercial batteries, as it penetrates and ultimately damages the graphite electrode. Oxidation and reduction of the liquid electrolyte at the electrodes during initial cycling results in the formation of the “solid-electrolyte interphase (SEI),”<sup>5–9</sup> consuming liquid electrolyte and incorporating some of the Li<sup>+</sup> charge carriers from the cell. This passivating layer is thought to grow until it has become sufficiently resistive to fully restrict electron transfer between the electrode and liquid electrolyte while allowing passage of Li<sup>+</sup>.<sup>3</sup> Thereafter, minimal damage occurs in the liquid electrolyte.

A great deal of effort has been dedicated to investigation of the electrodes and associated SEI of LIBs and the transport of Li<sup>+</sup> through these media.<sup>2,5,6,10–14</sup> Substantially less study has been directed towards the liquid electrolyte.<sup>15</sup> It is becoming

<sup>a</sup> Department of Chemistry, University of California, Berkeley, California 94720, USA. E-mail: saykally@berkeley.edu

<sup>b</sup> Chemical Sciences Division, Lawrence Berkeley National Laboratory, Berkeley, California 94720, USA

<sup>c</sup> Electrochemistry Branch, U.S. Army Research Laboratory, Adelphi, Maryland 20783, USA

<sup>d</sup> Materials Sciences Division, Lawrence Berkeley National Laboratory, Berkeley, California 94720, USA

<sup>e</sup> Molecular Foundry, Lawrence Berkeley National Laboratory, Berkeley, California 94720, USA

† Electronic supplementary information (ESI) available. See DOI: 10.1039/c4cp03240c



increasingly clear, however, that the structure of the liquid electrolyte substantially influences the function of LIBs, and that improvements to the liquid electrolyte are an essential component of the overall effort to improve LIBs for use in EVs and large-scale energy storage. Several studies have demonstrated that the solvation environment of the lithium ion in the electrolyte dictates the formation mechanism and resulting structure of the SEI.<sup>7,16–18</sup> This is significant for a number of reasons: SEI growth consumes  $\text{Li}^+$ , produces a high-resistivity region through which ions must migrate, and is widely implicated as the region of the battery in which failure is most likely to occur.<sup>19</sup> Furthermore, recent studies by Xu *et al.* have suggested that the desolvation of the  $\text{Li}^+$  from the liquid electrolyte is the slow step in  $\text{Li}^+$  insertion into the electrodes, thus comprising a critical limitation on power density and recharging rates.<sup>20,21</sup> Clearly, improvements in the electrolytic properties will improve nearly all significant aspects of LIB performance, including energy and power density, recharge time, and cycle life.

In order to realize the performance enhancements from improved electrolytes, it is necessary to thoroughly understand the electrolyte structure. Unfortunately, while a number of studies have been performed on LIB electrolyte systems, a clear picture of the solvation structure of the  $\text{Li}^+$  ion in alkyl carbonate solutions remains elusive. For example, several experimental and theoretical studies have suggested that a substantial degree of ion pairing/aggregation exists between  $\text{Li}^+$  and the counterion ( $\text{BF}_4^-$ ,  $\text{ClO}_4^-$ ,  $\text{PF}_6^-$ ) at concentrations of  $\sim 1$  M ( $1 \text{ mol/dm}^3$ ), the approximate solution concentration in standard commercial LIBs.<sup>22–25</sup> Other studies of the electrochemical properties and infrared and Raman spectra of the same solutions and concentrations have suggested little or no ion pairing or aggregation.<sup>16,26,27</sup> Similarly, the interactions of the ions with the solvent remain incompletely characterized. The generally favored structure comprises a tetrahedral coordination of carbonyl oxygen atoms around the  $\text{Li}^+$  and weakly solvated counterions. Numerous experimental and theoretical studies have found total coordination numbers for  $\text{Li}^+$  ( $\text{Li-O} + \text{Li-counterion interactions}$ ) very near four.<sup>8,25,28,29</sup> However, several vibrational spectroscopy studies (infrared absorption, Raman) of LIB electrolytes have suggested  $\text{Li}^+$  coordination numbers between 4 and 5.<sup>16,30,31</sup> A study published by Kondo *et al.* utilized conductivity measurements to estimate the coordination number of  $\text{Li}^+$  in PC at 4.3.<sup>27</sup> Neutron diffraction studies by Kameda *et al.* have found a Li–O coordination number of 4.5 in the same electrolyte solution.<sup>32</sup> Bogle *et al.* have interpreted the chemical shifts in  $^{17}\text{C}$  NMR to ascertain a Li–O coordination number of 5.69 for  $\text{LiPF}_6$  in EC,<sup>33</sup> while at least one study utilizing NMR diffusivity measurements has estimated a coordination number for  $\text{Li}^+$  as  $\text{LiClO}_4$  in EC to be  $\sim 7$  in concentrations up to  $\sim 1$  M.<sup>34</sup>

Here we investigate the coordination structure of  $\text{Li}^+$  in solutions of  $\text{LiBF}_4$  in PC using X-ray absorption spectroscopy (XAS) of liquid microjets.<sup>35</sup> XAS is an atom-specific core-level spectroscopic probe of the unoccupied electronic states; as such, it is sensitive to both the intra- and intermolecular environment of the target atom. Experimental spectra are interpreted through utilization of molecular dynamics simulations and spectral simulations

computed using the Prendergast–Galli excited electron and Core Hole (XCH) methodology.<sup>36</sup> Previous studies in our group have used these experimental and theoretical techniques to investigate the structure and chemistry of a variety of aqueous solutions.<sup>37–40</sup> Here, we extend the methodology to a non-aqueous system of substantial practical utility for the purpose of understanding and improving the solvation properties and desolvation process of the  $\text{Li}^+$  ion in LIB electrolytes.

## Experimental and theoretical methods

### a. X-ray spectroscopy of liquid microjets

$\text{LiBF}_4$  and PC were obtained from Sigma Aldrich and had minimum purity of 98% and 99.7%, respectively. PC was stored under dry nitrogen until use. X-ray absorption spectra were collected at Beamline 8.0.1 of the Advanced Light Source at Lawrence Berkeley National Laboratory (Berkeley, CA); this beamline has a nominal maximum output of  $6 \times 10^{15}$  photons/s with resolving power  $E/\Delta E$  of 7000. Liquid jets are produced by forcing pressurized ( $\sim 15$  bar) liquids through a  $100 \mu\text{m}$  inner diameter silica capillary into a vacuum chamber ( $10^{-5}$  Torr), where they interact with the X-ray beamline. Total electron yield (TEY) XA spectra are collected on a 2.1 kV biased copper as a function of photon energy. Our previous work has demonstrated that spectra obtained in this manner are representative of the bulk liquid.<sup>41,42</sup> Spectra are normalized to the signal collected simultaneously on a high-transmission gold grid intersecting the beamline several meters before it is focused into the chamber. Unlike previous work published by our group, this paper presents liquid spectra without gas-phase background subtraction; the low vapor pressure of PC ( $< 2$  Torr at 298 K) renders the gas phase spectrum insignificant, accounting for  $< 0.2\%$  of total intensity. Full XA spectra of the carbon and oxygen K-edges were collected with 0.2 eV step sizes and 1s count times; detailed spectra of the oxygen K-edge were collected with 0.05 eV steps and 2 s count times. Single-point energy axis calibrations were performed using gas-phase carbon dioxide for the carbon K-edge and liquid water for the oxygen K-edge. A more complete description of the experiment can be found in a prior publication.<sup>35</sup>

### b. Molecular dynamics simulations

A many-body polarizable force field (FF) APPLE&P<sup>43</sup> (Atomistic Polarizable Potential for Liquids, Electrolytes, and Polymers) has been used for molecular dynamics (MD) simulations of PC and (PC) $\text{LiBF}_4$  electrolytes. APPLE&P utilizes an exp-6 form for description of non-bonded interactions, also called the Buckingham potential, in conjunction with permanent charges situated on atomic sites and off-ether oxygen atomic sites for PC. The many-body polarization interactions are represented by the induced isotropic atomic dipoles and were solved self-consistently. The short-range interaction between induced dipoles is screened using Thole methodology with the Thole parameter ( $a_T = 0.4$ ). Atoms connected by bonds (1–2) and bends (1–2–3) were excluded from the list of non-bonded interactions. Atoms connected by 3 or more





bonds had full non-bonded interactions with the exception that 1–4 interaction between permanent charges and induced dipoles were scaled by 0.8. A detailed discussion of the functional form is provided elsewhere.<sup>43</sup> Previously developed PC and PC/Li<sup>+</sup> force field parameters were used.<sup>44,45</sup> APPLE&P parameters<sup>46</sup> for LiBF<sub>4</sub> were modified by refitting BF<sub>4</sub><sup>−</sup> charges to electrostatic potential around anion obtained at MP2/aug-cc-pVTz level, while Li··F repulsion parameters were refit to Li<sup>+</sup>/BF<sub>4</sub><sup>−</sup> binding energy obtained at the same level. The revised force field version was denoted as “e44.” The revised force field yielded ion self-diffusion coefficients and ionic conductivity of PC/LiBF<sub>4</sub> electrolytes in excellent agreement with experiments (available in ESI†).

We closely followed the simulation methodology previously used in MD simulations of electrolytes containing lithium salts.<sup>45,46</sup> Two PC–LiBF<sub>4</sub> systems have been constructed: a *large* simulation cell containing 640 PC and 64 LiBF<sub>4</sub>, and a *small* simulation cell containing 20 PC and 2 LiBF<sub>4</sub>. Simulations were performed at 298 K. Equilibration runs were 6 ns at 333 K followed by 3 ns and 6 ns equilibration runs in NPT ensemble at 298 K for the large and small systems, respectively. The density of the large box was imposed upon the small box to compensate for large density fluctuations arising from the small sample size. Production runs were performed for 8.3 ns and 1 ns for the large and small systems, respectively, in the NVT ensemble. The cutoff for non-bonded interactions was set to 12 Å for the large box and at half a box for the small simulation cell. Snapshots of the molecular configurations of the small simulation box were saved at 20 ps intervals for the spectral simulations. Snapshots from a small box containing 20 PC were generated following the same methods.

### c. Spectral simulations

Simulated spectra of the oxygen K-edge of PC and the (PC)LiBF<sub>4</sub> electrolyte were calculated using the XCH approximation,<sup>36</sup> a first-principles constrained-occupancy density functional theory (DFT) calculation, using molecular coordinates sampled from the small box MD simulations described above. DFT calculations were performed under periodic boundary conditions using the Plane Wave Self-Consistent Field (PWSCF) program within the Quantum-ESPRESSO package,<sup>47</sup> employing the Perdew–Burke–Ernzerhof form of the Generalized Gradient Approximation to the exchange–correlation potential.<sup>48</sup> The plane wave basis set, with a 25 Ry kinetic energy cutoff, is sufficiently flexible to model both localized and delocalized Kohn–Sham orbitals in the XCH approximation to the core-excited states. The electron density of the lowest energy core-excited state was generated self-consistently with explicit inclusion of a core hole on a target oxygen atom, modeled with a suitably modified pseudo-potential, together with the inclusion of the excited electron in the first available valence orbital. Higher energy excited states were approximated using the unoccupied Kohn–Sham orbitals of the XCH self-consistent field. Transition matrix elements were computed within Fermi’s golden rule between the 1s atomic orbital of the ground state and the unoccupied orbitals from the XCH calculation. Resulting transitions were broadened *via* Gaussian convolution using a fixed linewidth parameter of

0.2 eV to produce the final simulated spectrum. Spectra obtained from independent excited atoms and/or MD snapshots were aligned based on an isolated atomic reference, utilizing a previously-published methodology,<sup>39</sup> using the spectrum of gaseous CO<sub>2</sub> to provide a single-point energy alignment to experiment.

## Results and discussion

### a. XAS of PC and (PC)LiBF<sub>4</sub>

The TEY XA spectra collected for the carbon and oxygen K-edges of neat PC and 1 M LiBF<sub>4</sub> in PC are shown in Fig. 1 and 2, respectively. As the carbon K-edge spectrum exhibits no significant changes upon addition of the lithium salt, no additional analysis has been performed for these spectra. However, several features in the oxygen K-edge spectrum exhibit a blue shift in

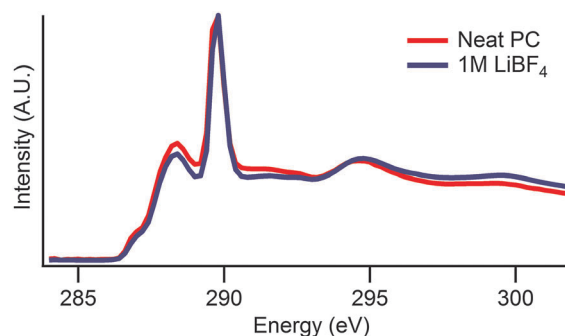


Fig. 1 Experimental carbon K-edge XAS spectra of propylene carbonate (PC) and 1 M (PC)LiBF<sub>4</sub>. The PC spectrum does not exhibit any significant change upon addition of the lithium salt.

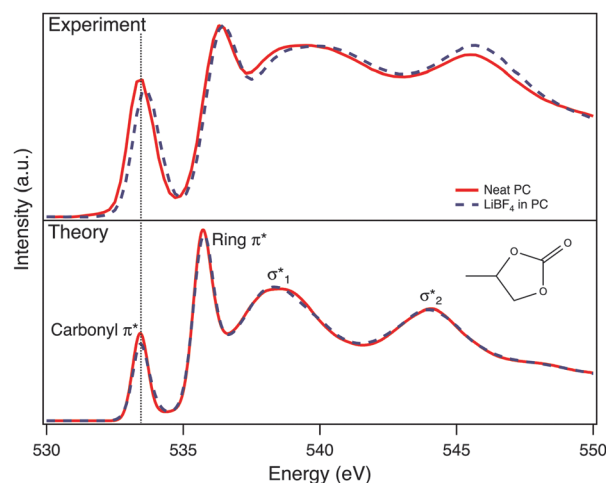


Fig. 2 Experimental and calculated oxygen K-edge XAS spectra of PC and (PC)LiBF<sub>4</sub>. The black dotted line corresponds to the center of a Gaussian fit performed on the carbonyl  $\pi^*$  feature of the experimental spectrum of neat PC. Features are labeled with their character as assigned from isosurfaces of the final states. The calculated PC spectrum accurately reproduces the experimental spectrum, but the blue shift observed in the experimental spectrum upon addition of LiBF<sub>4</sub> is not reproduced in the theory. The PC structure is illustrated in the lower panel.



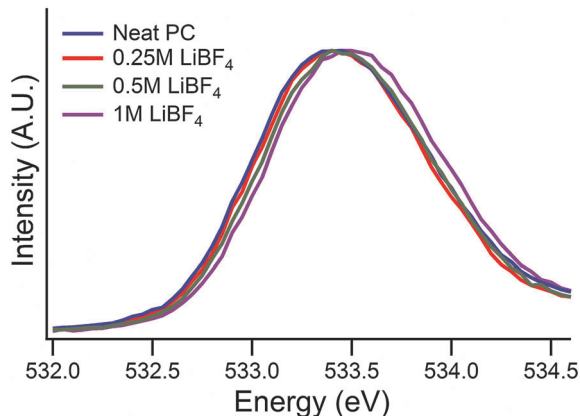


Fig. 3 High-resolution experimental XA spectra of the carbonyl  $\pi^*$  feature of PC and (PC)LiBF<sub>4</sub> electrolyte solutions. The blue shift observed for the  $\pi^*$  feature increases as a function of concentration: 0.25 M, 0.02 eV; 0.5 M, 0.04 eV; 1.0 M, 0.07 eV relative to neat PC.

the (PC)LiBF<sub>4</sub> electrolyte relative to the analogous features in the spectrum of the neat solvent. Detailed spectra on the first sharp feature in the oxygen K-edge spectra, near 533.5 eV, were collected for neat PC and solutions of 0.25, 0.5, and 1.0 M LiBF<sub>4</sub> in PC (Fig. 3). This feature exhibits a progressive blue shift, increasing as a function of LiBF<sub>4</sub> concentration, with a total shift of 0.07 eV from neat PC to the 1 M solution. As this spectral feature is much sharper and more clearly defined than those near 538 and 543 eV, which also exhibit blue shifts upon addition of the lithium salt, we have chosen to focus our analysis on this region of the spectrum.

### b. MD simulations

The large-box MD simulations produced values for diffusivity, conductivity, and degree of uncorrelated ionic motion (ionicity) in excellent agreement with previously reported experimental values;<sup>25</sup> these values are tabulated in the ESI.† A comparison of the structural parameters of the small and large boxes is presented in Fig. 4, with additional parameters found in the ESI.† The small box does exhibit a small increase in ion aggregation (Li<sup>+</sup>·F association number of 1.95 for the large box, 2.1 for the small box), likely facilitated by the enforced proximity of ions in the small box. The increase in Li<sup>+</sup>·BF<sub>4</sub><sup>-</sup> association is balanced by a corresponding decrease in the number of Li<sup>+</sup>-solvent interactions in the first solvation shell (2.3 large box, 2.15 small box), resulting in a constant value for the total lithium coordination number ( $\sim 4.25$ ). The Li<sup>+</sup>·carbonyl interaction lengths and Li<sup>+</sup>·O=C angular distributions are very similar for the small and large boxes (average Li<sup>+</sup>·O=C angle 149.2° large box, 148.4° small box). This suggests that the interactions between the lithium ion and solvent molecules are not substantially altered by the small system size in the small simulation box.

### c. Spectral simulations

Due to the high computational cost of performing first-principles electronic structure calculations on large systems,

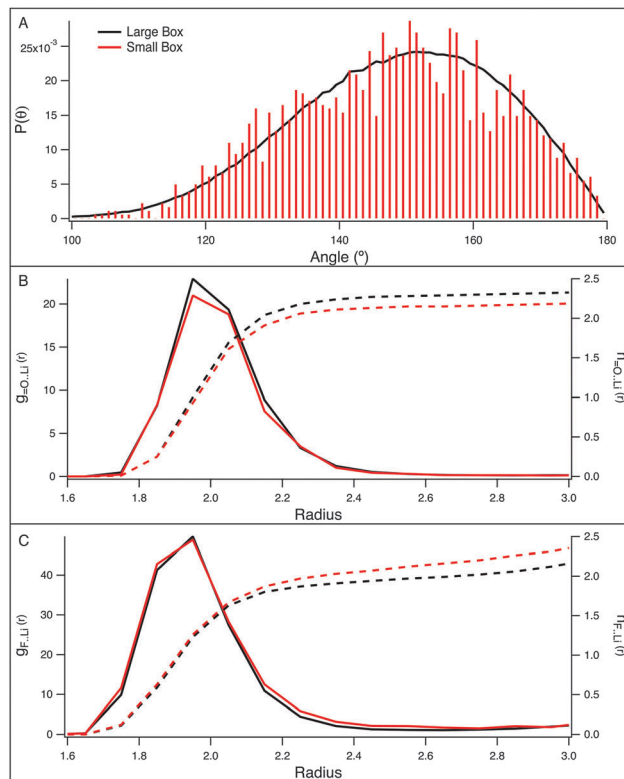


Fig. 4 Comparison of structural parameters from large (640 PC, 64 LiBF<sub>4</sub>) and small (20 PC, 2 LiBF<sub>4</sub>) MD simulation boxes: (a) angular distribution of Li<sup>+</sup>·O=C solvent interactions; (b) radial distribution functions (RDFs,  $g(r)$ ) and integrated radial distribution functions (IRDFs,  $n(r)$ ), shown as dashed lines) for interactions of Li<sup>+</sup> with PC carbonyl oxygen; and (c) RDFs and IRDFs for interaction of lithium with fluorine from the BF<sub>4</sub><sup>-</sup> counterion. There is a small increase in Li<sup>+</sup>·F interaction and decrease in Li<sup>+</sup>·O=C interaction in the small box relative to the large box, but the total coordination number (4.25) and solvent interaction angles are consistent.

the XCH calculation was performed using molecular configurations sampled from the small simulation boxes containing 20 PC for the neat liquid and 20 PC with 2 LiBF<sub>4</sub> for the electrolyte. The calculated spectrum of neat PC, shown in the bottom panel of Fig. 2, reproduces the experimental spectrum well. The calculated spectrum of the (PC)LiBF<sub>4</sub> electrolyte solution does not exhibit the characteristic blue shift relative to the neat liquid observed in the experimental spectrum. Observed transitions in the XA spectrum were assigned with the assistance of isosurfaces generated for the states comprising each of the four major spectral features in neat PC. These isosurfaces, presented in Fig. 5, suggest that the sharp features near 533.5 and 536.5 eV represent transitions to the  $\pi$ -antibonding system from the carbonyl and ring oxygen atoms, respectively. The broader, higher-energy states represent 1s- $\sigma^*$  transitions. As observed in the isosurfaces, the  $\sigma^*$  states are highly disperse, with substantial density on neighboring molecules; as such, configurational broadening arising from inhomogeneity of the liquid environment is the primary source of spectral broadening for these features. The  $\pi^*$  system is more localized, minimizing inhomogeneous broadening, explaining the narrower spectral width of features associated with transitions into this state.



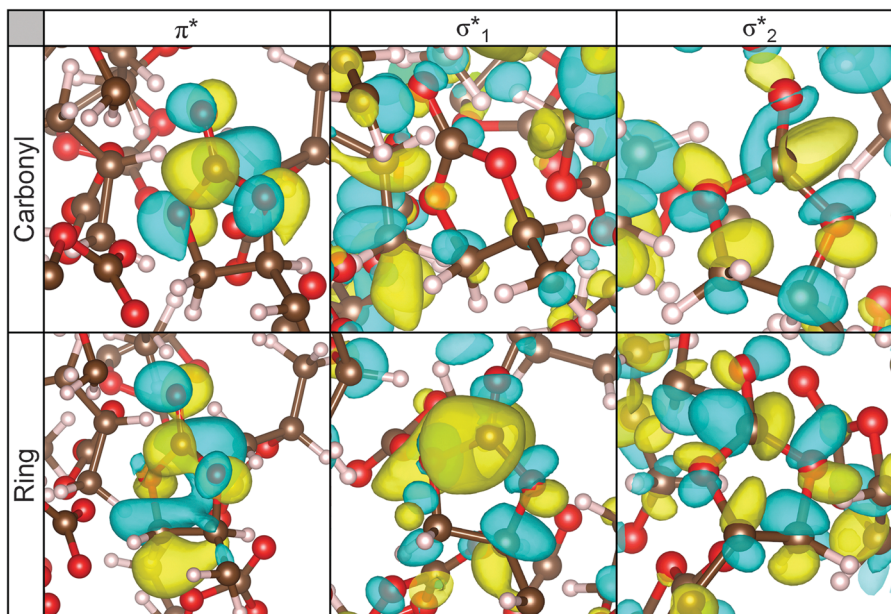


Fig. 5 Isosurfaces of excited states for transitions from the carbonyl and ring oxygen atoms of PC. All isosurfaces were calculated for the same molecule from the small simulation box of neat PC. Surfaces correspond to spectral features as labeled in Fig. 2. The  $\pi^*$  transitions originating from the carbonyl and ring oxygen atoms correspond to the separate, well-resolved transitions labeled as  $\pi^*$  carbonyl and  $\pi^*$  ring, while transitions from both the carbonyl and ring oxygen contribute to the spectral features denoted  $\sigma_1^*$  and  $\sigma_2^*$ . The  $\sigma^*$  states are highly delocalized throughout the neighboring PC molecules, resulting in substantial inhomogeneous configurational broadening of spectral features associated with transitions into these states. This phenomenon is not observed for the  $\pi^*$  transitions, which are observed to have far more localized excited states. Isosurfaces were generated using Quantum-ESPRESSO and visualized in VESTA.<sup>51</sup>

Other significant sources of broadening for these features include core-hole lifetime broadening and vibrational broadening.<sup>49</sup> In the condensed phase, vibrational structure is broadened, resulting in asymmetric features weighted towards the blue;<sup>50</sup> such structure is observed in the  $\pi^*$  features of the experimental spectra. Each  $\sigma^*$  feature contains spectral intensity for transitions originating from both carbonyl and ring oxygen atoms. While the calculated spectrum does not reproduce the experimental blue shift from PC to (PC)LiBF<sub>4</sub>, the features in the experimental spectrum exhibiting the shift originate at least in part from the carbonyl oxygen. The largest shift is observed in the carbonyl  $\pi^*$  feature. Less dramatic shifts are observed for the  $\sigma^*$  features, resulting from shifting only of the spectral lines associated with transitions originating from the carbonyl oxygen. The ring 1s to  $\pi^*$  transition exhibits very little shift in the experimental spectrum. These observations support the Raman findings of Kondo *et al.*, which suggest that Li<sup>+</sup>-PC interactions at concentrations below 2 M occur nearly exclusively at the carbonyl oxygen of PC.<sup>27</sup>

#### d. Evaluation of the Li<sup>+</sup>-PC coordination number

We divided the PC molecules in the molecular coordinates utilized to generate the calculated spectrum of PC(LiBF<sub>4</sub>) into two groups: those associating directly with the Li<sup>+</sup> ion (*i.e.* in the first solvation shell, Li<sup>+</sup>...O=C separation < 2.5 Å), and those not directly associating with Li<sup>+</sup> (free PC). Within the molecular coordinates sampled, no interactions were observed between Li<sup>+</sup> and PC except *via* the carbonyl oxygen; *i.e.* no ring oxygen or carbon atoms were located within the 2.5 Å interaction range.

The spectra calculated from excitations from the carbonyl and ring oxygen in the associating and non-associating molecule groups were averaged to produce independent spectra for PC

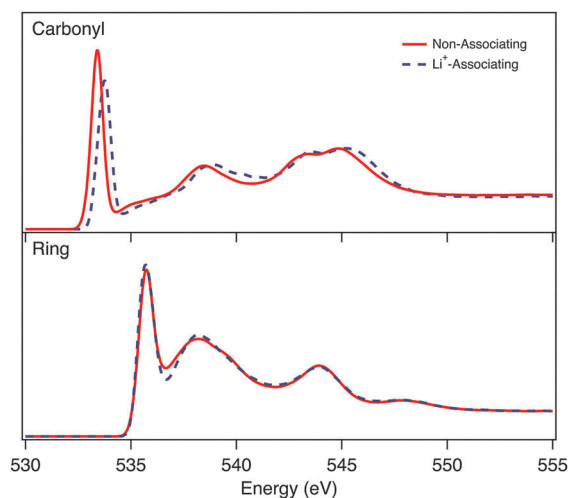


Fig. 6 Calculated XA spectra for transitions from carbonyl and ring oxygen in Li<sup>+</sup>-associating and non-associating PC molecules. 'Li<sup>+</sup>-associating' PC has been defined for the purposes of this distinction as having a Li<sup>+</sup> ion within 2.5 Å of the carbonyl oxygen; however, there are almost no Li<sup>+</sup>...O=C interactions longer than 2.25 Å and under 3 Å, as is apparent in the Li<sup>+</sup>...O=C RDF in Fig. 4. There is a distinct blue shift in the calculated XA spectrum of carbonyl oxygen interacting with lithium, while the spectrum of ring oxygen is insensitive to the presence of Li<sup>+</sup>. The calculated spectrum of non-interacting carbonyl oxygen closely matches the carbonyl oxygen spectrum of neat PC.





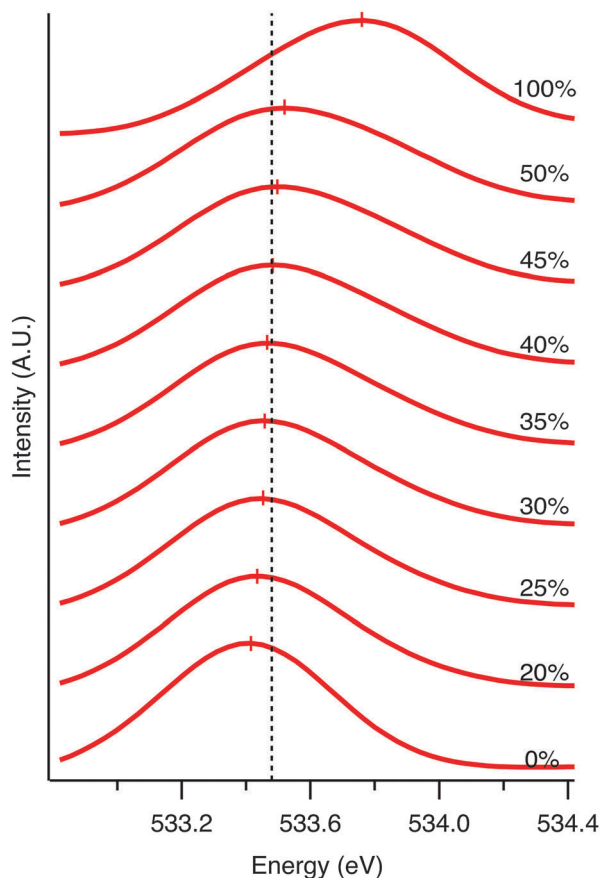


Fig. 7 Linear combinations of the calculated XA spectra of  $\text{Li}^+$ -associating and non-associating (free) PC molecules in  $(\text{PC})\text{LiBF}_4$  around the carbonyl  $\pi^*$  transition. Spectra are labeled with the weighting of  $\text{Li}^+$ -associating molecules in the linear combination producing each spectrum (thus, the curve labeled 0% is the spectrum of free PC, and 100% the spectrum of  $\text{Li}^+$ -associating PC). The center of each peak is marked with a vertical hash. The black dashed vertical line marks the experimental location of the carbonyl  $\pi^*$  transition in 1 M  $\text{LiBF}_4$ . The experimental peak is best reproduced by the linear combination comprising 40%  $\text{Li}^+$ -associating PC and 60% free PC.

associating with  $\text{Li}^+$  and free PC. These spectra are displayed in Fig. 6. As predicted, there is no substantive difference in the spectrum of ring oxygen between associating and non-associating molecules. However, the carbonyl oxygen spectrum of  $\text{Li}^+$ -associating PC molecules does exhibit a blue shift relative to that of free PC; for the carbonyl  $\pi^*$  feature centered at 533.5 eV, the peak is shifted by 0.35 eV, substantially greater than the experimental shift of 0.07 eV between the neat liquid and 1 M electrolyte solution. Thus, the inability of the initial theoretical calculations to reproduce the experimentally observed blue-shift most likely results from an underestimation of the association number of  $\text{Li}^+$ -PC in the MD simulations. In order to estimate the correct association number, we have generated linear combinations of the computed carbonyl oxygen XAS spectra of associating and non-associating carbonyl oxygen for ratios of 20–50% associating molecules. The carbonyl  $\pi^*$  region of these linearly combined spectra are presented in Fig. 7, along with a line indicating the location of the center of the carbonyl  $1s-\pi^*$  transition feature in

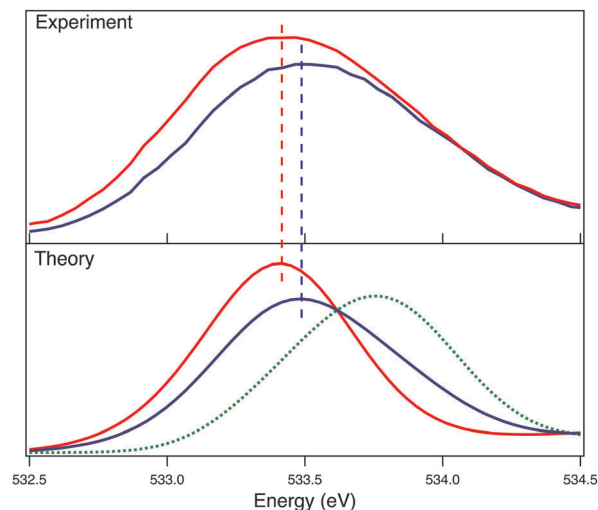


Fig. 8 Comparison of the calculated spectrum containing 40%  $\text{Li}^+$ -associating PC and 60% free PC with the experimental spectrum of 1 M  $\text{LiBF}_4$  in PC around the carbonyl  $\pi^*$  feature (in blue). The experimental spectrum of neat PC and calculated spectrum of non-associating PC molecules are shown in red for comparison. The dashed green line indicates the spectrum of the  $\text{Li}^+$ -associating PC molecules. This linear combination accurately reproduces the blue shift observed in the carbonyl  $\pi^*$  feature of the experimental XA spectrum of the  $(\text{PC})\text{LiBF}_4$  electrolyte relative to the neat liquid.

the experimental spectrum of 1 M  $\text{LiBF}_4$  in PC. The experimental shift is best reproduced by the combination containing 40% ( $\pm 2\%$ )  $\text{Li}^+$ -associating molecules. A comparison of the linear combination for this proportion of  $\text{Li}^+$ -associating PC to the experimental spectrum is shown in Fig. 8 and exhibits excellent agreement. Using a density of 1 M  $(\text{PC})\text{LiBF}_4$  of  $1.251 \text{ kg dm}^{-3}$ ,<sup>25</sup> this association proportion corresponds to an average  $\text{Li}^+$ -PC association number of 4.5 ( $\pm 0.2$ ). While incongruous with the standard tetrahedral model of  $\text{Li}^+$  solvation in electrolyte systems,<sup>8,25,28,29</sup> this value is in excellent agreement with that measured in neutron diffraction experiments<sup>32</sup> as well as IR studies of  $\text{Li}^+$ -EC.<sup>16</sup>

## Conclusions

The oxygen K-edge XA spectrum of PC exhibits a small blue shift upon addition of  $\text{LiBF}_4$  which increases as a function of concentration. Shifts are only observed in spectral features associated with transitions from the carbonyl oxygens; transitions from the ring oxygens are unaffected by the addition of salt. XCH calculations have shown that the spectrum of free PC in the electrolyte solution is unchanged from that of the neat liquid, while the spectra of PC molecules coordinating  $\text{Li}^+$  exhibit a blue shift. The experimental electrolyte spectrum can be accurately modeled as a linear combination of the spectra of  $\text{Li}^+$ -associating and free PC molecules. A linear combination of 40% lithium-associating and 60% free PC best reproduces the experimental spectrum of 1 M  $\text{LiBF}_4$ . From this ratio we have calculated a  $\text{Li}^+\cdots\text{O}=\text{C}$  association number of





$4.5 \pm 0.2$ . MD simulations developed to provide molecular coordinates for the XCH calculation produced bulk solution properties in good agreement with experimental values. However, on the molecular scale they underestimate the solvation number of  $\text{Li}^+$ -PC relative to the experimental value determined in this study. New theoretical investigations of LIB electrolyte solutions allowing for a substantial number of non-tetrahedral  $\text{Li}^+$  solvation structures will produce a more accurate model of the real solutions and may provide a route to improvements to current battery technology.

## Acknowledgements

This work was supported by facilities of the Lawrence Berkeley National Laboratory, the Advanced Light Source and National Energy Research Scientific Computing Center, supported by the Director, Office of Science, Office of Basic Energy Sciences, of the U.S. Department of Energy under Contract No. DE-AC02-05CH11231. The authors would like to acknowledge the excellent experimental support of all staff at the Advanced Light Source, with special thanks to Wanli Yang, Jonathan Spear, Alejandro Aguilar, and David Kilcoyne.

## References

- V. Narain, *Global Industrial Batteries Market*, Report, Frost & Sullivan, 2013.
- J. B. Goodenough and K.-S. Park, *J. Am. Chem. Soc.*, 2013, **135**, 1167–1176.
- J. B. Goodenough and Y. Kim, *Chem. Mater.*, 2010, **22**, 587–603.
- M. Armand and J.-M. Tarascon, *Nature*, 2008, **451**, 652–657.
- D. Aurbach, *J. Power Sources*, 2000, **89**, 206–218.
- E. Peled, *J. Electrochem. Soc.*, 1997, **144**, L208.
- P. Ganesh, P. R. C. Kent and D. Jiang, *J. Phys. Chem. C*, 2012, **116**, 24476–24481.
- K. Leung and J. L. Budzien, *Phys. Chem. Chem. Phys.*, 2010, **12**, 6583–6586.
- L. Xing, W. Li, C. Wang, F. Gu, M. Xu, C. Tan and J. Yi, *J. Phys. Chem. B*, 2009, **113**, 16596–16602.
- J. B. Goodenough, *Acc. Chem. Res.*, 2013, **46**, 1053–1061.
- I. Hung, L. Zhou, F. Pourpoint, C. P. Grey and Z. Gan, *J. Am. Chem. Soc.*, 2012, **134**, 1898–1901.
- S. J. Harris, A. Timmons, D. R. Baker and C. Monroe, *Chem. Phys. Lett.*, 2010, **485**, 265–274.
- O. Borodin, G. V. Zhuang, P. N. Ross and K. Xu, *J. Phys. Chem. C*, 2013, **117**, 7433–7444.
- O. Borodin and D. Bedrov, *J. Phys. Chem. C*, 2014, **118**, 18362–18371.
- K. Xu, *Chem. Rev.*, 2004, **104**, 4303–4417.
- M. Nie, D. P. Abraham, D. M. Seo, Y. Chen, A. Bose and B. L. Lucht, *J. Phys. Chem. C*, 2013, **117**, 25381–25389.
- A. von Cresce and K. Xu, *Electrochem. Solid-State Lett.*, 2011, **14**, A154.
- K. Xu, Y. Lam, S. S. Zhang, T. R. Jow and T. B. Curtis, *J. Phys. Chem. C*, 2007, **111**, 7411–7421.
- S. J. Harris and P. Lu, *J. Phys. Chem. C*, 2013, **117**, 6481–6492.
- K. Xu, A. von Cresce and U. Lee, *Langmuir*, 2010, **26**, 11538–11543.
- K. Xu and A. von Wald Cresce, *J. Mater. Res.*, 2012, **27**, 2327–2341.
- M. S. Ding, *J. Electrochem. Soc.*, 2004, **151**, A40.
- L. Yang, A. Xiao and B. L. Lucht, *J. Mol. Liq.*, 2010, **154**, 131–133.
- V. P. Reddy, M. C. Smart, K. B. Chin, B. V. Ratnakumar, S. Surampudi, J. Hu, P. Yan and G. K. Surya Prakash, *Electrochem. Solid-State Lett.*, 2005, **8**, A294.
- M. Takeuchi, Y. Kameda, Y. Umabayashi, S. Ogawa, T. Sonoda, S. Ishiguro, M. Fujita and M. Sano, *J. Mol. Liq.*, 2009, **148**, 99–108.
- C. M. Burba and R. Frech, *J. Phys. Chem. B*, 2005, **109**, 15161–15164.
- K. Kondo, M. Sano and A. Hiwara, *J. Phys. Chem. B*, 2000, **104**, 5040–5044.
- M. Morita, Y. Asai, N. Yoshimoto and M. Ishikawa, *J. Chem. Soc., Faraday Trans.*, 1998, **94**, 3451–3456.
- P. Ganesh, D. Jiang and P. R. C. Kent, *J. Phys. Chem. B*, 2011, **115**, 3085–3090.
- S.-A. Hyodo and K. Okabayashi, *Electrochim. Acta*, 1989, **34**, 1551–1556.
- J. L. Allen, O. Borodin, D. M. Seo and W. a. Henderson, *J. Power Sources*, 2014, **267**, 821–830.
- Y. Kameda, Y. Umabayashi, M. Takeuchi, M. A. Wahab, S. Fukuda, S. Ishiguro, M. Sasaki, Y. Amo and T. Usuki, *J. Phys. Chem. B*, 2007, **111**, 6104–6109.
- X. Bogle, R. Vazquez, S. Greenbaum, A. von W. Cresce and K. Xu, *J. Phys. Chem. Lett.*, 2013, **4**, 1664–1668.
- M. Castriota, E. Cazzanelli, I. Nicotera, L. Coppola, C. Oliviero and G. A. Ranieri, *J. Chem. Phys.*, 2003, **118**, 5537.
- K. R. Wilson, B. S. Rude, J. Smith, C. Cappa, D. T. Co, R. D. Schaller, M. Larsson, T. Catalano and R. J. Saykally, *Rev. Sci. Instrum.*, 2004, **75**, 725–736.
- D. Prendergast and G. Galli, *Phys. Rev. Lett.*, 2006, **96**, 215502.
- A. M. Duffin, A. H. England, C. P. Schwartz, J. S. Uejio, G. C. Dallinger, O. Shih, D. Prendergast and R. J. Saykally, *Phys. Chem. Chem. Phys.*, 2011, **13**, 17077–17083.
- A. M. Duffin, C. P. Schwartz, A. H. England, J. S. Uejio, D. Prendergast and R. J. Saykally, *J. Chem. Phys.*, 2011, **134**, 154503.
- A. H. England, A. M. Duffin, C. P. Schwartz, J. S. Uejio, D. Prendergast and R. J. Saykally, *Chem. Phys. Lett.*, 2011, **514**, 187–195.
- O. Shih, A. H. England, G. C. Dallinger, J. W. Smith, K. C. Duffey, R. C. Cohen, D. Prendergast and R. J. Saykally, *J. Chem. Phys.*, 2013, **139**, 035104.
- K. R. Wilson, B. S. Rude, T. Catalano, R. D. Schaller, J. G. Tobin, D. T. Co and R. J. Saykally, *J. Phys. Chem. B*, 2001, **105**, 3346–3349.
- C. D. Cappa, J. D. Smith, K. R. Wilson and R. J. Saykally, *J. Phys.: Condens. Matter*, 2008, **20**, 205105.



- 43 O. Borodin, *J. Phys. Chem. B*, 2009, **113**, 11463–11478.
- 44 A. von Wald Cresce, O. Borodin and K. Xu, *J. Phys. Chem. C*, 2012, **116**, 26111–26117.
- 45 O. Borodin and G. D. Smith, *J. Phys. Chem. B*, 2009, **113**, 1763–1776.
- 46 D. M. Seo, O. Borodin, S.-D. Han, P. D. Boyle and W. A. Henderson, *J. Electrochem. Soc.*, 2012, **159**, A1489–A1500.
- 47 P. Giannozzi, S. Baroni, N. Bonini, M. Calandra, R. Car, C. Cavazzoni, D. Ceresoli, G. L. Chiarotti, M. Cococcioni, I. Dabo, A. Dal Corso, S. de Gironcoli, S. Fabris, G. Fratesi, R. Gebauer, U. Gerstmann, C. Gougoussis, A. Kokalj, M. Lazzeri, L. Martin-Samos, N. Marzari, F. Mauri, R. Mazzarello, S. Paolini, A. Pasquarello, L. Paulatto, C. Sbraccia, S. Scandolo, G. Sclauzero, A. P. Seitsonen, A. Smogunov, P. Umari and R. M. Wentzcovitch, *J. Phys.: Condens. Matter*, 2009, **21**, 395502.
- 48 J. P. Perdew, K. Burke and M. Ernzerhof, *Phys. Rev. Lett.*, 1996, **77**, 3865–3868.
- 49 J. Stöhr, *NEXAFS Spectroscopy*, 1992, vol. 25.
- 50 C. P. Schwartz, J. S. Uejio, R. J. Saykally and D. Prendergast, *J. Chem. Phys.*, 2009, **130**, 184109.
- 51 K. Momma and F. Izumi, *J. Appl. Crystallogr.*, 2008, **41**, 653–658.

